PERIPHERAL NN-SCATTERING: ROLE OF DELTA-EXCITATION, CORRELATED TWO-PION AND VECTOR MESON EXCHANGE*

N. Kaiser, S. Gerstendörfer and W. Weise
Physik-Department, Technische Universität München,
D-85747 Garching, Germany

Abstract

We evaluate, within one-loop chiral perturbation theory, the two-pion exchange diagrams with single and double delta-isobar excitation contributing to elastic NN-scattering. We find that virtual Δ-excitation processes (in the static limit) produce the correct amount of isoscalar central attraction as needed in the peripheral partial waves with $L \geq 3$. Furthermore we compute the two-loop diagrams involving the $\pi\pi$-interaction (so-called correlated 2π-exchange). Contrary to common believe these processes lead to negligibly small and repulsive corrections to the NN-potential. The exchange of vector mesons (ρ, ω) turns out to be important for the F-wave phase shifts above $T_{lab} = 150$ MeV. Without adjustable parameters we are able to reproduce the empirical NN phase shifts up to 350 MeV for $L \geq 3$ and up to about (50–80) MeV for the D-waves. This is therefore the characteristic window in which the NN-interaction is basically governed by chiral symmetry. Not surprisingly, the lower partial waves require non-perturbative methods and additional short-distance parametrizations of the NN-dynamics.

*Work supported in part by BMBF.

I. INTRODUCTION AND SUMMARY

In a recent paper [1] we have developed a framework for the application of chiral perturbation theory to low energy elastic nucleon-nucleon scattering. In that framework a systematic expansion of the NN T-matrix in powers of small external momenta and quark masses is performed by evaluating tree and loop diagrams with vertices taken from an effective chiral Lagrangian. The latter is an efficient tool to implement the (chiral) symmetry constraints on the dynamics of pions (the Goldstone bosons of spontaneous chiral symmetry breaking in QCD). Since such an approach to NN-scattering focuses on the dynamics of pions it is expected to work within the kinematical domain where the NN force is dominated by one- and two-pion exchange. These are the peripheral NN partial waves below the inelastic $NN\pi$-threshold.

In ref. [1] the 2π-exchange contributions were worked out up to third order in small momenta including one-loop graphs with a vertex from the second order chiral πN-Lagrangian $\mathcal{L}^{(2)}_{\pi N}$. This part of the Lagrangian involves several additional low-energy constants c_i, $(i = 1, 2, 3, 4)$, which have been recently determined from a fit to many low energy pion-nucleon data [2]. Since some of these constants c_i are much larger than the natural scale $1/2M$ (M being the nucleon mass) they indeed produce the major 2π-exchange effect in NN-scattering. In particular, the isoscalar central potential is almost entirely given by the constant c_3 proportional to the so-called nucleon axial polarizability [2,3]. As shown in ref. [2] it is the $\Delta(1232)$-resonance that makes the dominant contribution to the low energy constants $c_{2,3,4}$ if one interprets their values in terms of resonance exchange. Therefore the 2π-exchange effects proportional to $c_{3,4}$ as calculated in ref. [1] can be approximately identified as single Δ-excitation graphs for which one has ignored the energy dependence of the Δ-propagator by using just a contact $\pi\pi NN$-vertex. However, at the inelastic $NN\pi$-threshold the nucleon kinetic energy T_{lab} becomes comparable to the ΔN-mass splitting of 293 MeV, and a treatment of important Δ-dynamics via contact interactions may be too crude. This is also indicated by the results in ref. [1] which show too large attraction in the F-waves above $T_{lab} = 180$ MeV and in the D-waves even for smaller energies around 50 MeV. One can expect that explicit $\Delta(1232)$ degrees of freedom cure this problem (at least partly).

In the past the Δ-excitation processes in NN-scattering have been considered in various approaches, either via dispersion theoretical methods [4] or using $N\Delta$-transition potentials [5–7] which neglect some (technically complicated) parts of the diagrams. At present no proper quantum field theoretical evaluation of these diagrams exists, which would avoid artificial "form factors" or cutoffs. As in ref. [8] such "form factors"are often introduced in order to enforce convergent loop integrals. In this work we evaluate the single and double Δ-excitation graphs in the static limit $M \to \infty$ (and also their first relativistic $1/M$-correction) using covariant perturbation theory and dimensional regularization. In one-loop order to which we are working here the divergences of the diagrams show up only as purely polynomial NN-amplitudes which do not contribute to the phase shifts with orbital angular momentum $L \geq 2$ and the mixing angles with $J \geq 2$. Therefore we can study the effects due to Δ-excitation in a completely parameterfree fashion.

Next we consider, at two-loop order, the two-pion exchange diagrams involving the chiral $\pi\pi$-interaction, so-called correlated 2π-exchange. In phenomenological approaches [4,5] such processes are often identified with the enhancement around masses of 550 MeV observed in the isoscalar central ($\pi\pi \to N\overline{N}$) spectral function proportional to $|f_{0+}|^2$.

Such a behavior is found in the dispersion theoretical analyses of the πN-scattering data [9] and often called "σ-meson". After transforming the respective NN-amplitudes into a local coordinate space potential, we find that these two-loop diagrams involving the chiral $\pi\pi$-interaction lead to rather different effects. In particular the resulting isoscalar central potential turns out to be weakly repulsive, contrary to common believe. The repulsive nature of isoscalar central potential finds its explanation in the isospin-zero S-wave $\pi\pi$-amplitude which becomes repulsive sufficiently far below the threshold. In any case, all effects due to correlated 2π-exchange (at two-loop) that we find here in (heavy baryon) chiral perturbation theory are in fact negligibly small. This means that the enhancement showing up in the spectral function $|f_{0+}|^2$ cannot simply be identified with the (perturbative two-loop) correlated 2π-exchange diagram.

With decreasing orbital angular momentum L we find that the description of the empirical F-wave NN phase shifts above $T_{lab} = 150$ MeV requires a further (well-known) ingredient, namely the exchange of vector mesons, ρ and ω. While ω-meson exchange (using $g^2_{\omega N}/4\pi = 12.9$ for its coupling constant) provides the necessary overall repulsion, the ρ-meson with its large tensor-to-vector coupling ratio ($\kappa_\rho = 6$) leads to the correct splitting of the singlet and the three triplet F-waves.

In D-waves we find deviations from the empirical NN phase shifts already at $T_{lab} = 100$ MeV (partly even for lower T_{lab}). For these low angular momentum partial waves the van der Waals behavior of the 2π-exchange NN-potential becomes problematic, since its r^{-6}-singularity practically extinguishes the natural centrifugal barrier effects coming from the wave function $r^2 j_2(pr)^2$ (with $j_2(pr)$ a spherical Bessel function). At such kinematics the short range NN-repulsion starts to become essential. Its dynamical origin lies of course outside the perturbative interaction of point-like baryons and mesons treated here. For some recent attempts on this problem in the framework of effective field theory see ref. [10,11]

We can summarize our work as follows: Within systematic perturbation theory based on chiral symmetry one finds an accurate description of the empirical NN phase shifts in the partial waves with $L \geq 3$ up to $T_{lab} = 350$ MeV and partly up to 80 MeV in D-waves with the following ingredients:

1) Point-like one-pion exchange (without introducing an unmeasurable πN form factor)

2) Iterated one-pion exchange

3) Irreducible two-pion exchange with only nucleons in intermediate states (plus their first relativistic $1/M$-correction)

4) Two-pion exchange with single and double Δ-isobar excitation (in the static limit)

5) Vector meson (ρ and ω) exchange with standard values of the coupling constants but no ad hoc form factors

These components comprise the dynamics of the peripheral nucleon-nucleon interaction. The emerging physical picture is of course not entirely new. However, our calculation is based on an effective chiral Lagrangian and we apply rigorous methods of perturbative quantum field theory (covariant Feynman graphs and dimensional regularization). Thus there is no need to introduce extra cut offs or ad hoc form factors which sometimes obscure the real physics.

On the experimental side there are upcoming precision data from the Indiana Cooler Synchrotron Facility (IUCF), which will lead to an improved NN phase shift analysis in the energy range below the pion production threshold. We propose to use the chiral NN phase shifts with $L \geq 3$ presented here as input in a future phase shift analysis.

II. BASIC FORMALISM

In this section, we briefly review some basic formalism needed to describe elastic nucleon-nucleon scattering. In the center of mass frame the on-shell T-matrix for the process $N(\vec{p}) + N(-\vec{p}) \to N(\vec{p}\,') + N(-\vec{p}\,')$ takes the following general form,

$$\begin{aligned}\mathcal{T}_{NN} = {} & V_C + \vec{\tau}_1 \cdot \vec{\tau}_2 W_C + [V_S + \vec{\tau}_1 \cdot \vec{\tau}_2 W_S]\, \vec{\sigma}_1 \cdot \vec{\sigma}_2 + [V_T + \vec{\tau}_1 \cdot \vec{\tau}_2 W_T]\, \vec{\sigma}_1 \cdot \vec{q}\, \vec{\sigma}_2 \cdot \vec{q} \\ & + [V_{SO} + \vec{\tau}_1 \cdot \vec{\tau}_2 W_{SO}]\, i(\vec{\sigma}_1 + \vec{\sigma}_2) \cdot (\vec{q} \times \vec{p}\,) \\ & + [V_Q + \vec{\tau}_1 \cdot \vec{\tau}_2 W_Q]\, \vec{\sigma}_1 \cdot (\vec{q} \times \vec{p}\,)\, \vec{\sigma}_2 \cdot (\vec{q} \times \vec{p}\,)\,. \end{aligned} \tag{1}$$

The ten complex functions $V_C, \ldots, W_Q$ depend on the center of mass momentum $p = |\vec{p}\,| = |\vec{p}\,'\,|$ and the momentum transfer $q = |\vec{q}\,|$ with $\vec{q} = \vec{p}\,' - \vec{p}$. The subscripts refer to the central, spin-spin, tensor, spin-orbit and quadratic spin-orbit components, each of which occurs in an isoscalar (V) and an isovector (W) version. In terms of the nucleon laboratory kinetic energy T_{lab} the center of mass momentum p is given as $p = \sqrt{T_{lab} M/2}$.

In order to compute the NN phase shifts and mixing angles one needs the matrix elements of $\mathcal{T}_{NN}$ in the LSJ-basis, where $L = J - S, J, J + S$, $S = 0, 1$ and $J = 0, 1, 2, \ldots$ denote the orbital angular momentum, the total spin and the total angular momentum respectively. The explicit form of the partial wave projection formulas can be found in section 3 of ref. [1]. Phase shifts and mixing angles are then given perturbatively as

$$\delta_{LSJ} = \frac{M^2 p}{4\pi E}\, \mathrm{Re}\, \langle LSJ | \mathcal{T}_{NN} | LSJ \rangle\,, \tag{2}$$

$$\epsilon_J = \frac{M^2 p}{4\pi E}\, \mathrm{Re}\, \langle J-1, 1J | \mathcal{T}_{NN} | J+1, 1J \rangle\,, \tag{3}$$

with the center of mass nucleon energy $E = \sqrt{M^2 + p^2}$. The perturbative expressions in eqs.(2,3) apply only if the phase shifts δ_{LSJ} and mixing angles ϵ_J are sufficiently small in order not to have any substantial violations of unitarity. We calculate reliably only those phase shifts and mixing angles which are smaller than 10° in magnitude. For these cases perturbation theory is well justified.

III. ONE LOOP DIAGRAMS WITH DELTA-EXCITATION

The one-loop diagrams with single and double Δ-isobar excitation are shown in Fig.1. The first diagram of triangle shape is specific for a calculation based on a chiral effective πN-Lagrangian, since it involves the Weinberg-Tomozawa isovector $NN\pi\pi$-contact vertex. Since all Feynman rules for the nucleon vertices and propagator are well documented in the recent review [12], we give here only some details associated with the Δ-isobar. In the heavy mass limit [13] where one considers the external momenta and the delta-nucleon mass splitting $\Delta = M_\Delta - M = 293$ MeV small compared to the nucleon mass, $M = 939$ MeV, one gets for the delta-propagator and the $\Delta \to \pi^a N$ transition vertex

$$\frac{i}{k_0 - \Delta + i0^+} \ , \qquad\qquad -\frac{3g_A}{2\sqrt{2}f_\pi}\vec{S}\cdot\vec{l}\,T_a \ . \tag{4}$$

Here k^μ denotes the four-momentum of the propagating delta (with its energy k_0 counted modulo the large nucleon mass M) and l^μ is the four-momentum of the emitted pion with isospin a. The 2×4 spin and isospin transition matrices S_i and T_a satisfy the relations $S_i\, S_j^\dagger = (2\delta_{ij} - i\epsilon_{ijk}\sigma_k)/3$ and $T_a\, T_b^\dagger = (2\delta_{ab} - i\epsilon_{abc}\tau_c)/3$ [14]. For the $\pi N\Delta$ coupling constant we have already inserted the large-N_c value $g_{\pi N\Delta} = 3g_{\pi N}/\sqrt{2}$ together with the Goldberger-Treiman relation $g_{\pi N} = g_A M/f_\pi = 13.4$ (with $f_\pi = 92.4$ MeV this gives $g_A = 1.32$). For the $\Delta \to \pi N$ decay width one finds in this case

$$\Gamma(\Delta \to \pi N) = \frac{3g_A^2}{32\pi f_\pi^2}\frac{E_N + M}{M + \Delta}(E_N^2 - M^2)^{3/2} = 110.6\,\mathrm{MeV}\,, \tag{5}$$

a number which is in good agreement with the empirical decay width $\Gamma(\Delta \to \pi N) = (115 \pm 5)$ MeV. Here $E_N = M + (\Delta^2 - m_\pi^2)/2M_\Delta = 966$ MeV denotes the center of mass energy of the decay nucleon. We note that eq.(5) for the Δ-decay width derives from a relativistic calculation using Rarita-Schwinger spinors [15]. Since the momentum of the decay pion is not so small, namely 227.3 MeV, one would loose important kinematical factors in a non-relativistic approximation and overestimate the Δ-decay width [14].

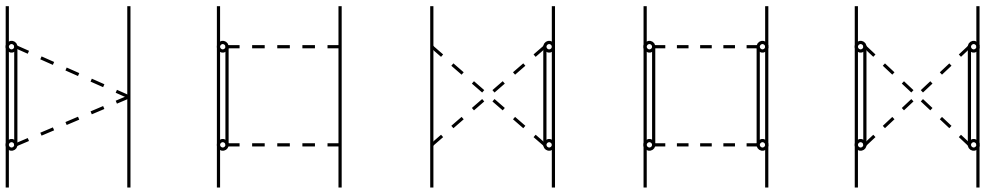

Fig.1: One-loop 2π-exchange diagrams with single and double $\Delta(1232)$-excitation

Now we give the one-loop NN-amplitudes which result from evaluating the diagrams shown in Fig.1 in the heavy mass limit, $M \to \infty$. For the sake of simplicity we omit purely polynomial terms which do not contribute to the phase shifts with $L \geq 2$ and to mixing angles with $J \geq 2$ (see section 4.1 in ref. [1]). The divergences of the loop diagrams are actually included in such (irrelevant) polynomial terms. We note that all one-loop vertex and self energy corrections with Δ-isobar excitation to the 1π-exchange diagram lead only to mass and coupling constant renormalization; they do not introduce a pion-nucleon "form factor" (see section 4.1 in [1]). We find the following analytical results for the three classes of diagrams shown in Fig.1:

a) Δ-excitation in triangle graphs:

$$W_C = \frac{g_A^2}{192\pi^2 f_\pi^4}\Big\{(6\Sigma - w^2)L(q) + 12\Delta^2\Sigma\, D(q)\Big\} \ . \tag{6}$$

b) Single Δ-excitation in box graphs:

$$V_C = \frac{3g_A^4}{32\pi f_\pi^4\Delta}(2m_\pi^2 + q^2)^2 A(q) \ , \tag{7}$$

$$W_C = \frac{g_A^4}{192\pi^2 f_\pi^4}\Big\{(12\Delta^2 - 20m_\pi^2 - 11q^2)L(q) + 6\Sigma^2\, D(q)\Big\} \ , \tag{8}$$

$$V_T = -\frac{1}{q^2}\, V_S = \frac{3g_A^4}{128\pi^2 f_\pi^4}\Big\{ -2L(q) + (w^2-4\Delta^2)D(q)\Big\}\ , \tag{9}$$

$$W_T = -\frac{1}{q^2}\, W_S = \frac{g_A^4}{128\pi f_\pi^4 \Delta} w^2 A(q)\ . \tag{10}$$

c) Double Δ-excitation in box graphs:

$$V_C = \frac{3g_A^4}{64\pi^2 f_\pi^4}\Big\{ -4\Delta^2 L(q) + \Sigma\,[H(q) + (\Sigma+8\Delta^2)D(q)]\Big\}\ , \tag{11}$$

$$W_C = \frac{g_A^4}{384\pi^2 f_\pi^4}\Big\{(12\Sigma - w^2)L(q) + 3\Sigma\,[H(q) + (8\Delta^2-\Sigma)D(q)]\Big\}\ , \tag{12}$$

$$V_T = -\frac{1}{q^2}\, V_S = \frac{3g_A^4}{512\pi^2 f_\pi^4}\Big\{6L(q) + (12\Delta^2 - w^2)D(q)\Big\}\ , \tag{13}$$

$$W_T = -\frac{1}{q^2}\, W_S = \frac{g_A^4}{1024\pi^2 f_\pi^4}\Big\{2L(q) + (4\Delta^2 + w^2)D(q)\Big\}\ . \tag{14}$$

The following set of loop functions and abbreviations has been used to express these NN-amplitudes,

$$L(q) = \frac{w}{q}\ln\frac{w+q}{2m_\pi}\ , \qquad w = \sqrt{4m_\pi^2+q^2}\ , \tag{15}$$

$$A(q) = \frac{1}{2q}\arctan\frac{q}{2m_\pi}\ , \tag{16}$$

$$D(q) = \frac{1}{\Delta}\int_{2m_\pi}^{\infty}\frac{d\mu}{\mu^2+q^2}\arctan\frac{\sqrt{\mu^2-4m_\pi^2}}{2\Delta}\ , \tag{17}$$

$$H(q) = \frac{2\,\Sigma}{w^2-4\Delta^2}\Big[L(q) - L(2\sqrt{\Delta^2-m_\pi^2})\Big]\ , \tag{18}$$

$$\Sigma = 2m_\pi^2 + q^2 - 2\Delta^2\ . \tag{19}$$

The isoscalar central V_C and isovector tensor amplitude W_T coming from the box graphs with single Δ-excitation in eqs.(7,10) show an interesting feature. The dependence on the delta-nucleon mass splitting Δ is a trivial factor Δ^{-1}. This means that, in the sum of the corresponding planar and crossed box graphs, the energy dependence of the delta-propagator has effectively disappeared. A $\pi\pi NN$-contact vertex ($-c_3 = 2c_4 = g_A^2/2\Delta$) proportional to the inverse mass splitting Δ^{-1} instead of the propagating Δ-isobars would give exactly the same result. Another way to understand this coincidence is to compute the sum of the energy denominators for all possible time-orderings which gives

$$\frac{2\omega_1\omega_2(\omega_1+\omega_2) + \Delta(\omega_1^2+3\omega_1\omega_2+\omega_2^2) + \Delta^2(\omega_1+\omega_2)}{\Delta\omega_1\omega_2(\omega_1+\omega_2)(\omega_1+\Delta)(\omega_2+\Delta)} \tag{20}$$

for the planar box graph and

$$\frac{\omega_1^2+\omega_1\omega_2+\omega_2^2+\Delta(\omega_1+\omega_2)}{\omega_1\omega_2(\omega_1+\omega_2)(\omega_1+\Delta)(\omega_2+\Delta)} \tag{21}$$

for the crossed box graph, with ω_1 and ω_2 denoting the on-shell energies of the two exchanged pions. The sum of the two expressions in eq.(20) and eq.(21) leads to the

surprisingly simple expression $2(\Delta\omega_1\omega_2)^{-1}$ in which the mass splitting Δ has factored out. In all other cases there is however a nontrivial dependence of the NN-amplitudes on the mass splitting Δ, in particular due to the occurrence of the loop function $D(q)$ for which we have given its spectral representation in eq.(17).

The NN-amplitudes in momentum space given above can be transformed into local coordinate space potentials (disregarding zero-range $\delta^3(\vec{r})$-terms) in the form of continuous superpositions of Yukawa functions (for details see section 6 in ref. [1]). The mass spectra entering in this representation are given by imaginary parts of the NN-amplitudes analytically continued to time-like momentum transfer $q = i\mu - 0^+$. This requires the knowledge of the imaginary parts of the loop functions for $\mu > 2m_\pi$,

$$L(i\mu) = \frac{\sqrt{\mu^2 - 4m_\pi^2}}{\mu}\Big[\ln\frac{\mu + \sqrt{\mu^2 - 4m_\pi^2}}{2m_\pi} - i\,\frac{\pi}{2}\Big]\,, \tag{22}$$

$$A(i\mu) = \frac{1}{4\mu}\Big[\ln\frac{\mu + 2m_\pi}{\mu - 2m_\pi} + i\,\pi\Big]\,, \tag{23}$$

$$\mathrm{Im}\,D(i\mu) = \frac{\pi}{2\mu\,\Delta}\arctan\frac{\sqrt{\mu^2 - 4m_\pi^2}}{2\Delta}\,. \tag{24}$$

Here we have also given the real parts of $L(i\mu)$ and $A(i\mu)$ which will be needed later in the discussion of the correlated two-pion exchange. As in our previous work [1] we will denote r-space potentials by a tilde, i.e. $\widetilde{V}_C(r)$ is the isoscalar central potential, etc.

The attractive isoscalar central potential $\widetilde{V}_C(r)$ generated by the Δ-excitation diagrams is shown in Fig.2. The main contribution comes from the four graphs with single Δ-excitation and it has the following simple analytical form

$$\begin{aligned}\widetilde{V}_C^{(N\Delta)}(r) &= -\frac{3g_A^4}{64\pi^2 f_\pi^4\Delta}\frac{e^{-2x}}{r^6}(6 + 12x + 10x^2 + 4x^3 + x^4) \\ &= -\frac{36}{\Delta}\Big\{2[\widetilde{W}_T^{(1\pi)}(r)]^2 + [\widetilde{W}_S^{(1\pi)}(r)]^2\Big\}\,,\end{aligned} \tag{25}$$

with the abbreviation $x = m_\pi r$. We have expressed this potential in the second line in terms of squares of the 1π-exchange isovector spin-spin and tensor potentials $\widetilde{W}_{S,T}^{(1\pi)}(r)$. For the isovector spin-spin and tensor potentials coming from the single Δ-excitation graphs one finds, similarly,

$$\begin{aligned}\widetilde{W}_S^{(N\Delta)}(r) &= \frac{g_A^4}{192\pi^2 f_\pi^4\Delta}\frac{e^{-2x}}{r^6}(1 + x)(3 + 3x + 2x^2) \\ &= \frac{4}{\Delta}\Big\{[\widetilde{W}_T^{(1\pi)}(r)]^2 - [\widetilde{W}_S^{(1\pi)}(r)]^2\Big\}\,,\end{aligned} \tag{26}$$

$$\begin{aligned}\widetilde{W}_T^{(N\Delta)}(r) &= -\frac{g_A^4}{192\pi^2 f_\pi^4\Delta}\frac{e^{-2x}}{r^6}(1 + x)(3 + 3x + x^2) \\ &= \frac{4}{\Delta}\widetilde{W}_T^{(1\pi)}(r)\Big\{\widetilde{W}_S^{(1\pi)}(r) - \widetilde{W}_T^{(1\pi)}(r)\Big\}\,.\end{aligned} \tag{27}$$

The relative weights between the 1π-exchange spin-spin and tensor potential in eqs.(25,26,27) can be easily understood from relations between the tensor operator $S_{12}(\hat{r}) = 3\vec{\sigma}\cdot\hat{r}\,\vec{\sigma}_2\cdot\hat{r} - \vec{\sigma}_1\cdot\vec{\sigma}_2$ and the spin-spin operator $\vec{\sigma}_1\cdot\vec{\sigma}_2$. These relations are: $[S_{12}(\hat{r})]^2 = 6 + 2\vec{\sigma}_1\cdot\vec{\sigma}_2 - 2S_{12}(\hat{r})$, $\{S_{12}(\hat{r}), \vec{\sigma}_1\cdot\vec{\sigma}_2\} = 2S_{12}(\hat{r})$ and $(\vec{\sigma}_1\cdot\vec{\sigma}_2)^2 = 3 - 2\vec{\sigma}_1\cdot\vec{\sigma}_2$.

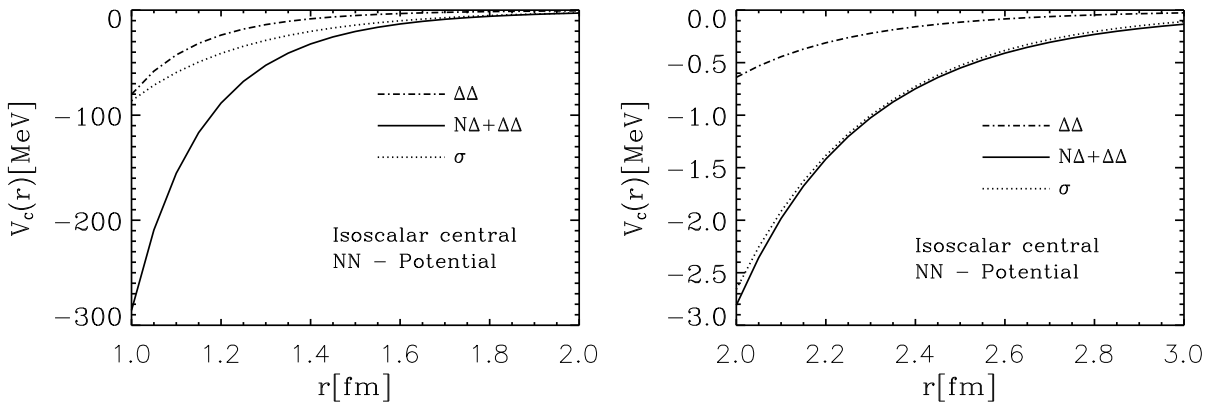

Fig.2: The isoscalar central NN-potential $\widetilde{V}_C(r)$ generated by 2π-exchange with $\Delta(1232)$-excitation versus the nucleon distance r.

Note that the relevant energy difference $\Delta/12 = 24.4$ MeV in eq.(25) is rather small. It is quite remarkable that these simple relations between $\widetilde{V}_C^{(N\Delta)}(r)$, $\widetilde{W}_{S,T}^{(N\Delta)}(r)$ and the 1π-exchange potentials (eq.(25,26,27)) are exact for the isoscalar central and the isovector spin-spin/tensor potentials generated by the direct and crossed box graph with single Δ-excitation (in the static limit $M \to \infty$). Heuristic considerations already suggest such a form of the isoscalar central 2π-exchange potential.

The double Δ-excitation diagrams amount to about 30% of the total isoscalar central potential as shown by the dashed-dotted line in Fig.2. The fictitious "σ"-exchange potential $\widetilde{V}_C^{(\sigma)}(r) = -(g_\sigma^2/4\pi r)e^{-M_\sigma r}$ with $g_\sigma^2/4\pi = 7.1$ and $M_\sigma = 550$ MeV [8] is also shown in Fig.2 by the dotted line. For distances $r > 2$ fm one observes an almost perfect agreement between the phenomenological "σ"-exchange potential and the total isoscalar central potential generated by 2π-exchange with Δ-excitation. For shorter distances $r < 2$ fm the latter one increases more strongly in magnitude due to its inherent r^{-6}-singularity (van der Waals behavior). Among all potentials generated by Δ-excitation the isoscalar central $\widetilde{V}_C(r)$ is by far the largest one. The attractive isovector central potential $\widetilde{W}_C(r)$ is approximately a factor ten smaller, with values of -32.7 MeV, -2.0 MeV and -0.25 MeV at distances $r = 1$ fm, 1.5 fm and 2.0 fm. The repulsive isoscalar and isovector spin-spin potentials $\widetilde{V}_S(r)$, $\widetilde{W}_S(r)$ and the attractive isoscalar and isovector tensor potentials $\widetilde{V}_T(r)$, $\widetilde{W}_T(r)$ are even smaller, with typical values of ± 13 MeV at $r = 1$ fm. The asymptotic behavior for large r is $e^{-2m_\pi r}r^{-5/2}$ for the isovector central potential $\widetilde{W}_C(r)$ and $e^{-2m_\pi r}r^{-7/2}$ for the isoscalar spin-spin/tensor potential $\widetilde{V}_{S,T}(r)$. In the other cases it can be read off from eqs.(25,26,27). We note that throughout the large-r asymptotics is determined alone by the box graphs with single Δ-excitation b).

We have furthermore evaluated the first relativistic correction, proportional to $1/M$, to the Δ-excitation graphs starting from the Rarita-Schwinger form of the spin-3/2 propagator and $\pi N\Delta$-vertex. Explicit formulas for the respective NN-amplitudes can be found in the appendix. Unfortunately these corrections are not small in the range 1 fm $< r <$ 2 fm or for $T_{lab} > 100$ MeV. The reason is probably found in combinatoric factors (up to six vertices and propagators are expanded in powers of $1/M$) and in the fact that the ratio $\Delta/M \simeq 0.3$ is not so small. We expect that part of these relativistic $1/M$-corrections will

be cancelled by higher orders in the $1/M$-expansion. On the other hand it is not clear how realistic a description of the Δ-resonance via a local Rarita-Schwinger spinor-field really is, even though it is the only available Lorentz-covariant formalism for spin-3/2 particles [16]. Off its mass-shell the Rarita-Schwinger spinor-field exhibits potentially unphysical spin-1/2 degrees of freedom. In view of these problems we prefer not to include the relativistic $1/M$-correction to the Δ-excitation graphs (Fig.1) in our calculation.

Let us give another argument in support of the idea that the Δ-excitation in the static limit ($M \to \infty$) already represents the low energy $\pi\pi \to N\overline{N}$ dynamics in the scalar isoscalar channel quite well. The shift of the nucleon scalar form factor $\sigma_N(t)$ from momentum transfer $t = 0$ to $t = 2m_\pi^2$ has been evaluated in ref. [17] via dispersion relations and empirical πN- and $\pi\pi$-data. The result is $\sigma_N(2m_\pi^2) - \sigma_N(0) = 15.2 \pm 0.4$ MeV. In the one-loop approximation of heavy baryon chiral perturbation theory one finds for this scalar-isoscalar quantity [18],

$$\sigma_N(2m_\pi^2) - \sigma_N(0) = \frac{3g_A^2 m_\pi^2}{64\pi^2 f_\pi^2}\Big\{\pi\, m_\pi - 4\sqrt{\Delta^2 - m_\pi^2}\,\ln\frac{\Delta + \sqrt{\Delta^2 - m_\pi^2}}{m_\pi} + (\pi - 4)\Delta + 8\Delta^3\, D(i\sqrt{2}m_\pi)\Big\} = (8.0 + 6.9)\,\text{MeV} \tag{28}$$

where the first term $\sim \pi m_\pi$ comes from the pion loop-diagram with a nucleon intermediate state, and the remaining ones come from an analogous diagram with an intermediate $\Delta(1232)$-isobar ($8\Delta^2 D(i\sqrt{2}m_\pi) = 7.02$). The sum 14.9 MeV of both terms agrees well with the dispersion-theoretical value 15.2 ± 0.4 MeV. While the detailed spectral function $\mathrm{Im}\,\sigma_N(t)$ given by these two one-loop diagrams is not in perfect agreement [18] with the empirical one derived via dispersion theory [17], the relevant integral over $\mathrm{Im}\,\sigma_N(t)/t(t - 2m_\pi^2)$ is well reproduced.

We expect a similar mechanism to be at work for the 2π-exchange isoscalar central NN-potential which can anyhow only be tested at large and intermediate distances, $r > 1.5$ fm. The mass spectrum $\mathrm{Im}\,V_C$ as given by the Δ-excitation diagrams in the static limit does certainly not have all structures as the one derived from dispersion theory [4,9], in particular there is no enhancement around 550 MeV (the broad "σ"-meson). By analogy with the previous discussion of the nucleon scalar form factor we expect that the long and intermediate range components of the isoscalar central potential $\widetilde{V}_C(r)$ are well represented by the Δ-excitation graphs in the static limit. For the long and intermediate range isoscalar central potential only the low energy part and some global features, but not the details of its mass spectrum, play a role. The good agreement between the "σ"-potential and the Δ-excitation 2π-exchange potential for $r > 2$ fm in Fig.2 demonstrates this fact very clearly.

IV. CORRELATED TWO-PION EXCHANGE

As previously mentioned the mass spectrum in the isoscalar central channel $\mathrm{Im}\,V_C \sim |f_{0+}|^2$, with the $\pi\pi \to N\overline{N}$ S-wave amplitude f_{0+}, shows an enhancement around 550 MeV (the so-called "σ"-meson) [4,9]. This enhancement is often interpreted as originating from correlated two-pion exchange (the first diagram shown in Fig.3) in which the two exchanged pions interact while propagating between the two nucleons. This motivated us to evaluate this specific two-loop diagram in heavy baryon chiral perturbation theory.

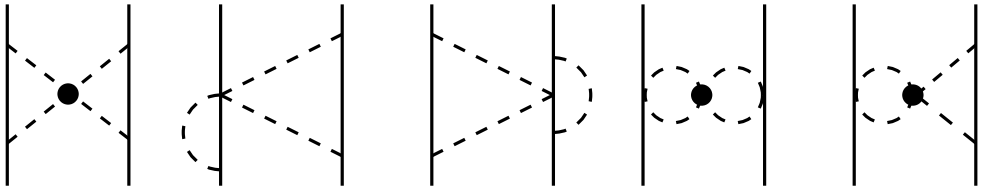

Fig.3: Correlated two-pion exchange diagrams and some related two-loop graphs. The dot represents the $\pi\pi$-interaction

The correlated 2π-exchange diagram involves the off-shell $\pi\pi$-interaction which is, however, not uniquely defined by the effective chiral Lagrangian. It depends on the choice of the interpolating pion field or, to be explicit, on the parametrization of the SU(2)-matrix $U(\vec{\pi}\,)$ which is the basic variable entering the non-linear chiral $\pi\pi$-Lagrangian,

$$U(\vec{\pi}\,) = 1 + \frac{i}{f_\pi}\vec{\tau}\cdot\vec{\pi} - \frac{1}{2f_\pi^2}\vec{\pi}^{\,2} - \frac{i\,\alpha}{f_\pi^3}(\vec{\tau}\cdot\vec{\pi}\,)^3 + \frac{\alpha-\frac{1}{8}}{f_\pi^4}\vec{\pi}^{\,4} + \ldots \tag{29}$$

The arbitrariness of the coefficient α in the 3rd and 4th power of the pion field just reflects this ambiguity. For the pure, isolated $\pi\pi$-interaction this does not cause a problem since the off-shell amplitude $A_{\pi\pi} = (s_{\pi\pi}-m_\pi^2+2\alpha(4m_\pi^2-q_1^2-q_2^2-q_3^2-q_4^2))/f_\pi^2$ is not an observable and the on-shell amplitude can be easily shown to be independent of α. However, the isoscalar central NN-amplitude V_C generated by the first diagram in Fig.3 is α-dependent. It is therefore not meaningful to consider this diagram alone, instead one has to find the complete subclass of diagrams for which the unphysical α-dependence drops out. This subclass is obtained by adding those diagrams which result from shifting the 4π-vertex to a nucleon line (see a typical representative in Fig.3). This procedure resembles the construction of gauge invariant subclasses. The four additional diagrams now indeed cancel an unwanted term proportional to $10\alpha - 1$. We note that for isovector amplitudes there is no α-dependence in the first diagram of Fig.3. Altogether we find the following contribution to the NN T-matrix from the factorizable two-loop diagrams in Fig.3:

$$V_C = -\frac{3g_A^4}{1024\pi^2 f_\pi^6}(m_\pi^2+2q^2)\Big[m_\pi + (2m_\pi^2+q^2)A(q)\Big]^2\,, \tag{30}$$

$$\begin{aligned} W_C = -\frac{1}{18432\pi^4 f_\pi^6}\Big\{&\Big[4m_\pi^2(1+2g_A^2)+q^2(1+5g_A^2)\Big]L(q) \\ &-4m_\pi^2(1+2g_A^2)+q^2(1+5g_A^2)\ln\frac{m_\pi}{\lambda} - \frac{q^2}{6}(5+13g_A^2)\Big\}^2\,, \end{aligned} \tag{31}$$

$$W_T = -\frac{1}{q^2}\,W_S = -\frac{g_A^4}{2048\pi^2 f_\pi^6}\Big[m_\pi + w^2 A(q)\Big]^2\,. \tag{32}$$

Note that V_C and W_T are finite in dimensional regularization. The divergent terms in W_C have been omitted according to the usual minimal subtraction prescription which introduces a logarithmic dependence on the renormalization scale λ. The expressions in eqs.(30,31,32) for correlated 2π-exchange in heavy baryon chiral perturbation theory have a simple interpretation in terms of the one-loop contributions to the nucleon scalar and isovector electromagnetic form factors [19]:

$$V_C = \frac{32\pi}{3m_\pi^4} t_0^0(-q^2)\Big[\sigma_N(-q^2)_{\rm loop}\Big]^2 \ , \tag{33}$$

$$W_C = -\frac{1}{8f_\pi^2}\Big[G_E^V(-q^2)_{\rm loop}\Big]^2 \ , \tag{34}$$

$$W_T = -\frac{1}{q^2}\, W_S = -\frac{1}{32M^2 f_\pi^2}\Big[G_M^V(-q^2)_{\rm loop}\Big]^2 \ . \tag{35}$$

with $t_0^0(s_{\pi\pi}) = (2s_{\pi\pi} - m_\pi^2)/(32\pi f_\pi^2)$ the on-mass-shell isospin-zero S-wave $\pi\pi$-amplitude at leading order. Actually, we have considered for W_C a larger class of factorizable two-loop graphs as shown in Fig.3, such that no additive constant to the electric from factor $G_E^V(-q^2)_{\rm loop}$ appears under the square in eq.(34). Note that both central NN-amplitudes in eqs.(33,34) are negative which indicates a repulsive NN-interaction. The negative sign of V_C comes from the isospin-zero S-wave $\pi\pi$-amplitude evaluated at negative $s_{\pi\pi} = -q^2 < 0$. As a matter of fact chiral soft pion theorems require the $\pi\pi$-interaction to be of derivative-nature which unavoidably leads to strong energy dependence of the isospin-zero S-wave amplitude. An immediate consequence is that the attractive isospin-zero S-wave $\pi\pi$-interaction above threshold ($s_{\pi\pi} \geq 4m_\pi^2$) switches over to repulsion sufficiently far below the threshold ($s_{\pi\pi} < 0$). In the NN-scattering process the exchanged pion pair belongs exclusively to the latter kinematical region $s_{\pi\pi} < 0$. This is the basic reason why we find here a (weakly) repulsive isoscalar central potential from correlated 2π-exchange.

r[fm]	1.0	1.5	2.0	$r \to 0$	$r \to \infty$
$\widetilde{V}_C$	0.731	0.090	0.016	r^{-4}	$e^{-2m_\pi r} r^{-2} \ln r$
$\widetilde{W}_C$	3.811	0.571	0.092	$r^{-7} \ln r$	$e^{-2m_\pi r} r^{-5/2}$
$\widetilde{W}_S$	–0.170	–0.022	–0.004	r^{-4}	$e^{-2m_\pi r} r^{-3}$
$\widetilde{W}_T$	0.193	0.022	0.004	r^{-4}	$e^{-2m_\pi r} r^{-3}$

Tab.1: Coordinate space potentials from correlated 2π-exchange in units of MeV.

In Tab.1 we display some values for the coordinate space potentials as they derive from our calculation of the correlated 2π-exchange using the corresponding imaginary parts ($\mathrm{Im}\,[A(i\mu)]^2 = 2\,\mathrm{Re}\,A(i\mu)\,\mathrm{Im}\,A(i\mu)$ etc.) to evaluate their spectral representations [1]. In order to get an estimate of the magnitude of $\widetilde{W}_C(r)$ we set $\lambda = M_\omega = 782$ MeV. Indeed both central potentials and the tensor potential are repulsive but they are also negligibly small. We have confirmed this furthermore by evaluating the contribution of the NN-amplitudes in eqs.(30,31,32) to the phase shifts and mixing angles. In the case of the correlated 2π-exchange isovector spin-spin potential one can even give an expression in closed form,

$$\widetilde{W}_S(r) = \frac{g_A^4}{6144\pi^3 f_\pi^6}\frac{e^{-2x}}{r^7}\Big\{(15+30x+24x^2+8x^3)(\gamma_E + \ln 4x) \\ +(15-30x+24x^2-8x^3)e^{4x}E_1(4x) - 4x(15+15x+8x^2+2x^3)\Big\} \ , \tag{36}$$

with $x = m_\pi r$, $\gamma_E = 0.5772...$ the Euler-Mascheroni number and $E_1(4x) = \int_{4x}^\infty d\zeta \zeta^{-1} e^{-\zeta}$ the exponential integral function. The isovector spin-spin potential $\widetilde{W}_S(r)$ in eq.(36)

has only a r^{-4}-singularity near the origin and it vanishes identically in the chiral limit, $m_\pi = 0$. The isoscalar central potential $\widetilde{V}_C(r)$ and the isovector tensor potential $\widetilde{W}_T(r)$ from correlated 2π-exchange have actually the same features. In contrast to this the isovector central potential $\widetilde{W}_C(r)$ from correlated 2π-exchange does not vanish in the chiral limit $m_\pi = 0$ and it has a much stronger $r^{-7}\ln r$-singularity near the origin. In Tab.1 the asymptotic behavior for large r is also given.

In ref. [8] further correlated 2π-exchange diagrams with single and double Δ-excitation were considered. We restrict ourselves here to a rough estimate of their effects. Obviously the contribution of the diagrams with Δ-excitation is overestimated in the limit of zero mass splitting, $\Delta = 0$. In that case only different spin/isospin factors show up in comparison with the diagrams involving nucleon intermediate states. The isoscalar central amplitude V_C in eq.(30) would simply be multiplied by a factor 9. Comparing with the scalar form factor difference $\sigma_N(2m_\pi^2) - \sigma_N(0)$ where the Δ-isobar in the zero mass splitting limit triples the pure nucleon-term, one expects an amplification factor around 4 to be a more realistic estimate of Δ-effects for finite mass splitting. In the case of the isovector tensor amplitude W_T the degenerate Δ-isobars would lead to a factor 9/4 in eq.(32), and for the isovector central amplitude W_C the g_A-dependent terms in eq.(31) would be cancelled by degenerate Δ-isobars. Even including such amplification factors due to intermediate Δ-isobars the correlated 2π-exchange is a negligibly small correction. This completes the discussion of the correlated 2π-exchange in heavy baryon chiral perturbation theory. As a main result we find that this diagram cannot be identified with the enhancement showing up in the empirical isoscalar central spectral function $|f_{0+}|^2$. Analogous features have already been observed in the one-loop calculation of the πN scattering amplitude in ref. [2]. There the (class of) diagrams with pion self-interaction reduces the spin- and isospin averaged P-wave scattering volume P_1^+ as well as the nucleon axial polarizability α_A. A reduction of these quantities is just the opposite of what one naively expects from scalar-isoscalar $\pi\pi$-correlations.

V. VECTOR MESON EXCHANGE

It is clear that the coupling of vector mesons (ρ, ω) to nucleons has no direct relation to chiral symmetry. The vector meson mass scale actually marks the kinematical endpoint of chiral dynamics with weakly interacting pions. However, vector mesons are an important ingredient for the understanding of nucleon structure, as witnessed e.g. by the dispersion-theoretical analysis of the nucleon electromagnetic form factors [9,20] and the successful one-boson-exchange models of the NN-interaction [8]. In our study of the peripheral NN phases we find that the chiral 2π-exchange considered so far is insufficient to describe the empirical F-wave phase shifts above $T_{lab} = 150$ MeV (see Fig.4 in our previous work [1]). The source of the discrepancy is a much too strong attraction between the nucleons for distances $r < 1.5$ fm. Naturally one expects that vector meson exchange produces the repulsive interaction at intermediate distances which will be able to cure this problem.

The coupling of the ρ- and ω-meson to the nucleon is characterized by vector coupling constants $g_{\rho N,\omega N}$ and tensor-to-vector coupling ratios $\kappa_{\rho,\omega}$. We will apply symmetry relations to minimize the number of free vector meson parameters. The KSFR relation $M_\rho = M_\omega = \sqrt{2} g_\rho f_\pi = 782$ MeV leads to $g_\rho = 6.0$ for the universal ρ-coupling constant. Via isospin considerations one obtains $g_{\rho N} = g_\rho/2 = 3.0$ and SU(3) symmetry would pre-

dict $g_{\omega N}^{SU(3)} = 3g_\rho/2$. However, all existing determinations of $g_{\omega N}$ point towards a larger value. We use here $g_{\omega N} = \sqrt{2} g_{\omega N}^{SU(3)} = 12.7$ as obtained from a global fit of the NN F-waves. This number is in the range of values found from forward NN-dispersion relations [21] ($g_{\omega N} = 10.1 \pm 0.9$), the Bonn NN-potential [8] ($g_{\omega N} = 11.5$) and the recent dispersion analysis of the nucleon electromagnetic form factors [20] ($g_{\omega N} = 20.9 \pm 0.3$). For the tensor-to-vector coupling ratio we use the values of ref. [8], $\kappa_\rho = 6$ and $\kappa_\omega = 0$, which are also confirmed by the nucleon electromagnetic form factor analysis of [20] ($\kappa_\rho = 6.1 \pm 0.2$, $\kappa_\omega = -0.16 \pm 0.02$). The precise value of κ_ω is irrelevant for the NN F-wave phase shifts as long as it is sufficiently small, $|\kappa_\omega| < 0.2$. The ρ-meson exchange between two nucleons leads to the following isovector NN-amplitudes,

$$W_C = -\frac{g_{\rho N}^2}{4M^2(M_\rho^2+q^2)}\Big\{\Big[2E - \frac{q^2}{2}\Big(\frac{1}{E+M} + \frac{\kappa_\rho}{M}\Big)\Big]^2 + (4p^2-q^2)\Big(\frac{\kappa_\rho q^2}{4M(E+M)} - 1\Big)^2\Big\}\,, \tag{37}$$

$$W_T = -\frac{1}{q^2}\,W_S = -\frac{g_{\rho N}^2(1+\kappa_\rho)^2}{4M^2(M_\rho^2+q^2)}\,, \tag{38}$$

$$W_{SO} = -\frac{g_{\rho N}^2}{4M^2(M_\rho^2+q^2)}\Big\{\Big[2E - \frac{q^2}{2}\Big(\frac{1}{E+M} + \frac{\kappa_\rho}{M}\Big)\Big]\Big(\frac{1}{E+M} + \frac{\kappa_\rho}{M}\Big) + \Big[1 + \kappa_\rho\Big(\frac{E}{M} - \frac{q^2}{4M(E+M)}\Big)\Big]\Big(2 - \frac{\kappa_\rho q^2}{2M(E+M)}\Big)\Big\}\,, \tag{39}$$

$$W_Q = -\frac{g_{\rho N}^2}{4M^2(M_\rho^2+q^2)}\Big\{\frac{(4p^2-q^2)\kappa_\rho^2}{4M^2(E+M)^2} - \Big(\frac{1}{E+M} + \frac{\kappa_\rho}{M}\Big)^2 - \frac{2\kappa_\rho}{M(E+M)}\Big[1 + \kappa_\rho\Big(\frac{E}{M} - \frac{q^2}{4M(E+M)}\Big)\Big]\Big\}\,, \tag{40}$$

where we have kept the fully relativistic expressions ($E = \sqrt{M^2+p^2}$). In a non-relativistic truncation at order M^{-2} one would otherwise loose important contributions, in particular the quadratic spin-orbit term W_Q proportional to the large coefficient $2\kappa_\rho^2 + 2\kappa_\rho + 1/4$. Interestingly, the fully relativistic tensor and spin-spin terms $W_{T,S}$ in eq.(38) agree exactly with the lowest order non-relativistic approximation. For a pseudoscalar meson exchange this is also the case [1]. The isoscalar NN-amplitudes due to ω-exchange are obtained in complete analogy by the replacement $(g_{\rho N}, \kappa_\rho) \to (g_{\omega N}, \kappa_\omega)$ in eqs.(37-40). For ω-exchange (with $\kappa_\omega \simeq 0$) the truncation at order M^{-2} is sufficiently accurate. At energies where ρ- and ω-exchange are important it is not meaningful to approximate them by local (polynomial) contact terms, since the ratio q/M_ω is not small.

For the sake of completeness one should also add the exchange of η-mesons with mass $m_\eta = 547.45$ MeV. In the absence of a reliable empirical determination of the ηN-coupling constant $g_{\eta N}$ we will use the SU(3)-value $g_{\eta N} = (3F-D)M/\sqrt{3}f_\pi = 4.4$ together with the approximate values of the octet axial vector coupling constants $D = 3/4$ and $F = 1/2$. For comparison the Bonn OBE-model (without 2π-exchange) uses $g_{\eta N} = 6.8$. The η-exchange leads to an isoscalar tensor amplitude of the form,

$$V_T = \frac{3}{64 f_\pi^2 (m_\eta^2 + q^2)}\,. \tag{41}$$

The actual calculation of the phase shifts shows that η-exchange with the coupling strength given by SU(3) is almost negligible in all partial waves with $L \geq 2$. We have furthermore evaluated the $K\overline{K}$-exchange (bubble and triangle) diagrams in heavy baryon chiral perturbation theory. As expected these processes lead to very small repulsive isoscalar and isovector central NN-potentials, $\widetilde{V}_C(1\,\mathrm{fm}) = 0.99$ MeV, $\widetilde{W}_C(1\,\mathrm{fm}) = 0.26$ MeV.

VI. RESULTS FOR PHASE SHIFTS AND MIXING ANGLES

In this section we present and discuss our results for the NN phase-shifts with $L \geq 3$ and mixing angles with $J \geq 3$ up to nucleon laboratory kinetic energies of $T_{lab} = 350$ MeV. For the D-wave phase shifts and ϵ_2 we show results only up to $T_{lab} = 120$ MeV. First, we state all ingredients which go into the calculation. We include all terms derived in the recent work [1], the point-like 1π-exchange, the iterated 1π-exchange and the irreducible 2π-exchange with the low energy constants $c_{1,3,4}$ set equal to zero. The terms proportional to $c_{3,4}$ are now substituted by explicit $\Delta(1232)$-dynamics, and c_1 gave anyhow only a marginal contribution to the isoscalar central amplitude V_C. The new ingredients are the 2π-exchange with Δ-excitation in the static limit (section 3) and the vector meson exchange (section 5) with coupling constants $g_{\rho N} = 3$, $\kappa_\rho = 6$, $g_{\omega N} = 12.7$, $\kappa_\omega = 0$. We use throughout the value $m_\pi = 138$ MeV for the (average) pion mass.

A. D-WAVES

The D-wave phase shifts and mixing angle ϵ_2 are shown in Fig.4 up to $T_{lab} = 120$ MeV. The dashed curve corresponds to the one-pion exchange approximation and the full curve includes in addition two-pion exchange and vector meson exchange. The dotted curve represents the recent empirical energy dependent NN phase shift analysis of ref. [22] (VPI). The triangles and squares give NN phase shifts and mixing angles derived from single energy analyses of ref. [23] and ref. [22], respectively. The circles represent the results of the multi-energy partial wave analysis of ref. [24] (Tab.IV,V). In all cases the two-pion and vector meson exchange corrections go into the right direction, but deviations show up already above $T_{lab} = 30$ MeV in the ${}^1D_2$ partial wave and above $T_{lab} = 50$ MeV for ${}^3D_1$ and ${}^3D_3$. The ${}^3D_2$ phase shift and the mixing angle ϵ_2 are in agreement with the data up to $T_{lab} = 100$ MeV. Similar results were found recently in ref. [25] using a somewhat different approach to the 2π-exchange. Compared to our previous calculation [1], there is no improvement in the D-wave phase shifts and ϵ_2 due to adding (perturbative) ρ- and ω-exchange. The 2π-exchange with its r^{-6} singular behavior still provides too large attraction at distances $r \leq 1$ fm. Obviously, the D-wave phase shifts and ϵ_2 above $T_{lab} = 100$ MeV are already sensitive to the short range NN-repulsion beyond ω-exchange. It appears, that the D-waves (above $T_{lab} = 100$ MeV), as well as the S- and P-waves, require non-perturbative methods and phenomenological parametrizations of the short range NN-interaction. This is, of course, well known from earlier investigations.

B. F-WAVES

The F-wave phase shifts and the mixing angle ϵ_3 are shown in Fig.5. We present here results up to $T_{lab} = 350$ MeV, i.e. 70 MeV above the $NN\pi$-threshold where inelasticities

are still negligible. The phase shifts in the $^1F_3$, $^3F_2$, $^3F_3$ partial waves are in very good agreement with the empirical data up to $T_{lab} = 350$ MeV, whereas deviations show up in the $^3F_4$ partial wave above $T_{lab} = 220$ MeV. The good agreement in the former case results from the inclusion of ρ- and ω-exchange. The ω-exchange compensates the too strong attraction from to 2π-exchange. The ρ-exchange with its large tensor, spin-orbit and quadratic spin-orbit amplitudes ($\kappa_\rho = 6$) leads to the correct splitting of the singlet and the three triplet F-wave phase shifts. In particular, the correct downward bending of the $^3F_2$ phase shift is a vector meson exchange effect (see Fig.4 in [1] where the opposite behavior was found from 2π-exchange alone). The deviation in the $^3F_4$ partial wave above $T_{lab} = 220$ MeV suggests that further short range effects are at work in this particular channel. The mixing angle ϵ_3 is in perfect agreement with the data for all energies up to $T_{lab} = 350$ MeV. Irreducible 2π-exchange and iterated 1π-exchange contribute to this quantity with roughly equal strength. There is also a small but non-negligible contribution from vector meson exchange to ϵ_3 above $T_{lab} = 200$ MeV.

C. G-WAVES

The G-wave phase shifts and the mixing angle ϵ_4 are shown in Fig.6. The predictions are in good agreement with the data for all four partial wave phase shifts, and with the mixing angle up to $T_{lab} = 350$ MeV. The vector mesons ρ and ω almost do not operate anymore in these high angular momentum states, $L = 4$. At $T_{lab} = 300$ MeV they produce phase shift contributions of 0.3° and smaller. One has now reached the chiral window in which 1π- and (chiral) 2π-exchange describe the NN-interaction completely and reliably. Note that the differences between 1π-exchange and data are still sizeable in the $^1G_4$ and $^3G_5$ partial waves. The chiral 2π-exchange closes this gap between the data and the 1π-exchange approximation. In the $^1G_4$ partial wave the correction comes mainly from irreducible 2π-exchange, whereas in the $^3G_5$ partial wave (with total isospin $I = 0$) both irreducible 2π-exchange and iterated 1π-exchange contribute with roughly equal strength. Compared to our previous calculation [1] the (very small) $^3G_5$ phase shift does not bend over to positive values any more. For the $^3G_3$ and $^3G_4$ phase shifts and ϵ_4 the 2π-exchange corrections are relatively small. Nevertheless, these small effects improve the agreement between data and chiral predictions.

D. H-WAVES

The H-wave phase shifts and the mixing angle ϵ_5 are shown in Fig.7. The $^1H_5$ phase shift and the mixing angle ϵ_5 have converged to the 1π-exchange approximation. In the $^3H_4$ and $^3H_5$ partial wave one finds small corrections to 1π-exchange which nevertheless improve the agreement with the empirical data. Note however that the 1π-exchange approximation considerably underestimates the empirical $^3H_6$ phase shifts. Again this gap is closed by the chiral 2π-exchange. It is rather remarkable that the 2π-exchange effects are still important at such a large orbital angular momentum, $L = 5$.

E. I-WAVES

The I-wave phase shifts and the mixing angle ϵ_6 are shown in Fig.8. Again, the $^3I_6$ phase shift and the mixing angle ϵ_6 have converged to the 1π-exchange. In the $^1I_6$, $^3I_5$ and $^3I_7$ partial waves we predict small differences to the empirical phases of ref. [22]. The calculation presented here is indeed most reliable in the high angular momentum partial waves.

F. INTERACTION DENSITIES

In order to learn about the relevant length scales at which the peripheral NN interaction actually takes place it is most instructive to study the local interaction densities. These are expressions of the form $r^2 j_L(pr)^2 \widetilde{U}_{LSJ}(r)$, with $j_L(pr)$ a spherical Bessel function and $\widetilde{U}_{LSJ}(r)$ the coordinate space potential in a given state $|LSJ\rangle$. Unfortunately, a fully equivalent representation of the phase shifts δ_{LSJ} and the mixing angles ϵ_J in terms of local interaction densities is not possible because of some inherent non-localities of the iterated 1π-exchange (section 4.3 in ref. [1]) and the quadratic spin-orbit interaction. Nevertheless, the generic features are already displayed by the dominant contributions to the NN T-matrix, namely 1π-exchange and the isoscalar central components of 2π- and ω-exchange. Two examples of such interaction densities are shown in Fig.9 for the $^3F_4$ partial wave at $T_{lab} = 200$ MeV and the $^1G_4$ partial wave at $T_{lab} = 250$ MeV. One can clearly see the peaking of the interaction densities around distances of about $r = 1.5$ fm and $r = 2.5$ fm, respectively. It results on one side from the centrifugal barrier effect given by the wave function $r^2 j_L(pr)^2$ and on the other side from the exponential decay of the potential $\widetilde{U}_{LSJ}(r)$. Varying the orbital angular momentum L and the center of mass momentum p, the peak of the interaction density moves and appears approximately at a distance $r \approx L/p$. This length scale corresponds just to the classical impact parameter.

VII. CONCLUDING REMARKS

The chiral perturbation theory calculation of the NN phase shifts and mixing angles, presented here, is most reliable in the high angular momentum partial waves which probe the long and medium range parts of the NN force. This is the region where 1π- and 2π-exchange explains the NN-interaction in a model independent way. We have demonstrated that the S- and P-wave chiral dynamics of the pion-nucleon system determines the peripheral NN phase shifts almost completely, with no arbitrary cutoffs or "form factors". The new aspect emphasized in this work is that the chiral pion-baryon effective Lagrangian provides a well-defined systematic framework to deal with the peripheral nucleon-nucleon interaction. In particular there is no need to introduce the scalar-isoscalar "σ"-meson. The intermediate range isoscalar central attraction is explicitly produced by van der Waals-type 2π-exchange including intermediate Δ-isobar excitations. Effects from $\pi\pi$-rescattering turn out to be negligibly small, in accordance with the suppression of higher loops in chiral perturbation theory.

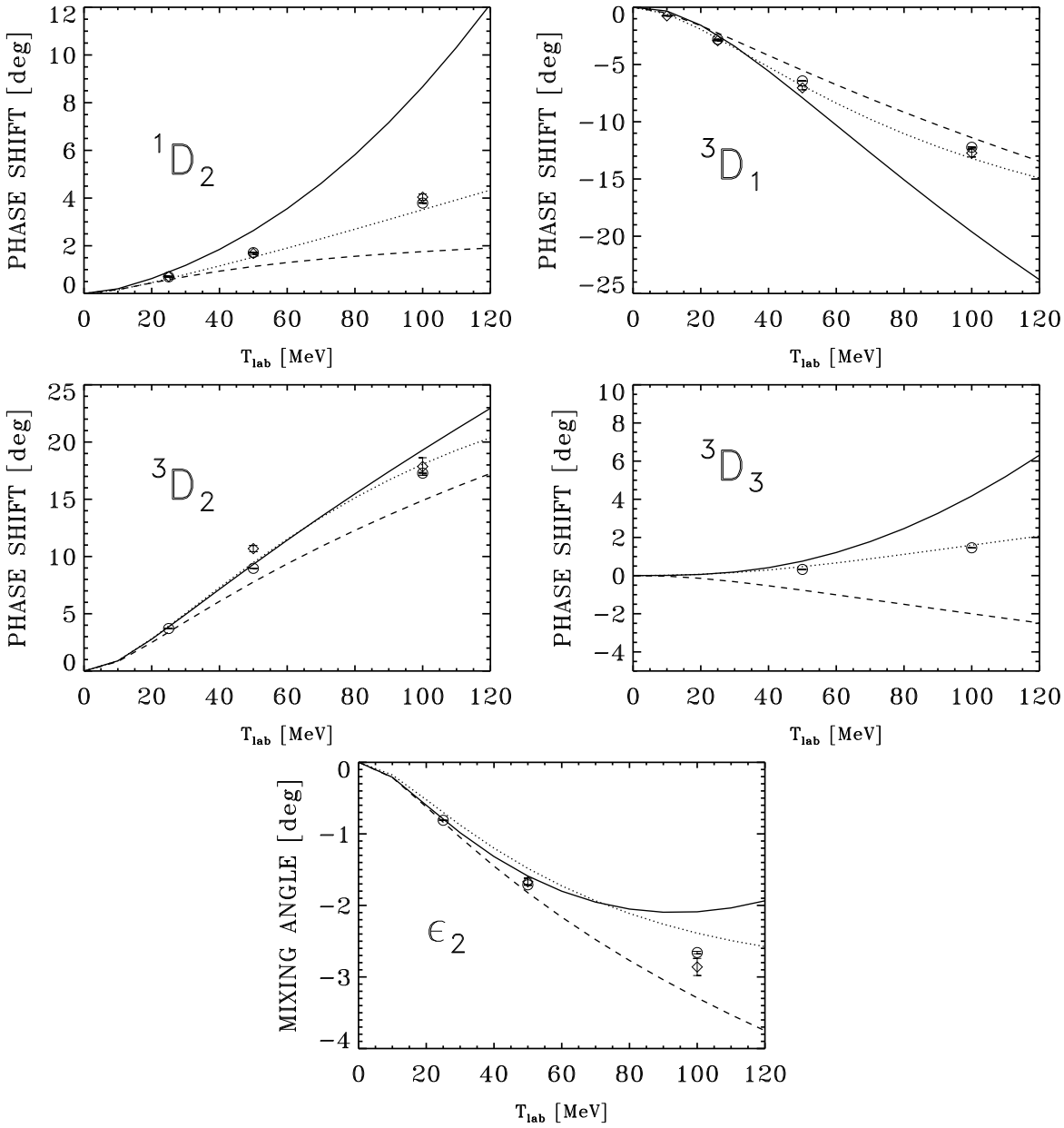

Fig.4: D-wave NN phase shifts and mixing angle ϵ_2 versus the nucleon laboratory kinetic energy T_{lab}. The dashed curves correspond to the 1π-exchange approximation and the full curves include chiral 2π- and vector meson exchange as well. The dotted curves represent the empirical energy dependent NN phase shift analysis of ref. [22].

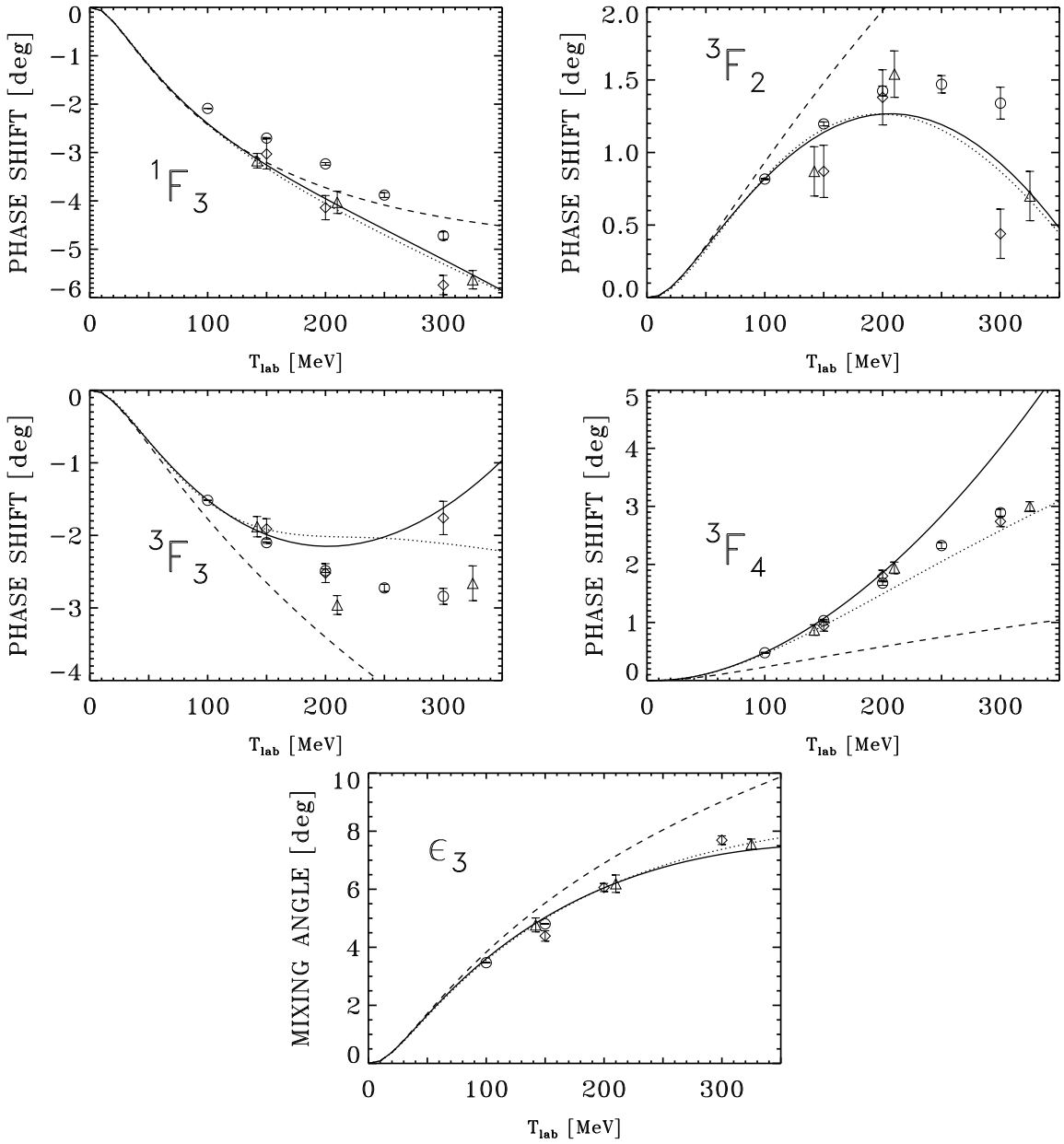

Fig.5: F-wave NN phase shifts and mixing angle ϵ_3 versus the nucleon laboratory kinetic energy T_{lab}. For notations see Fig.4.

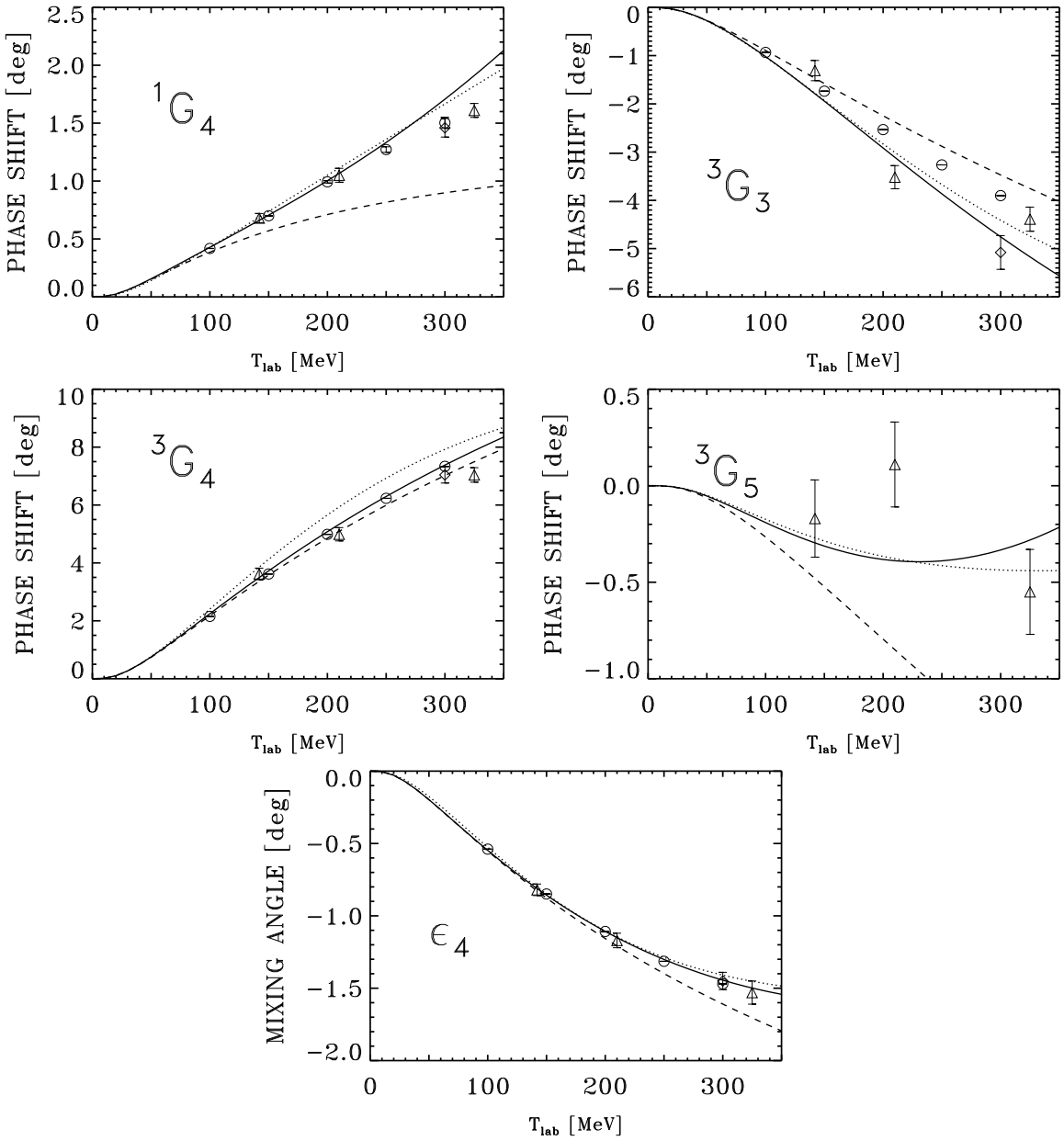

Fig.6: G-wave NN phase shifts and mixing angle ϵ_4 versus the nucleon laboratory kinetic energy T_{lab}. For notations see Fig.4.

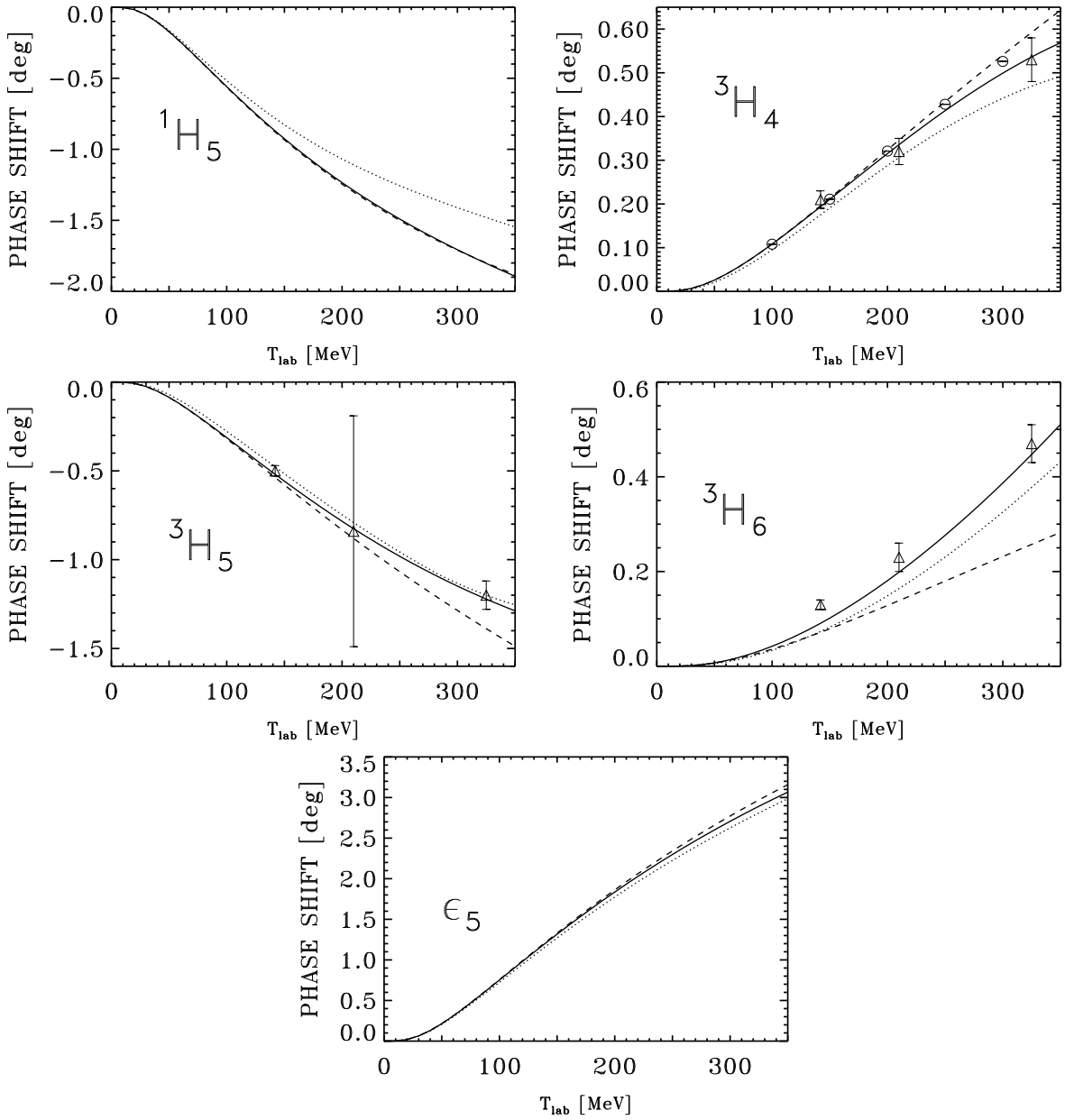

Fig.7: H-wave NN phase shifts and mixing angle ϵ_5 versus the nucleon laboratory kinetic energy T_{lab}. For notations see Fig.4.

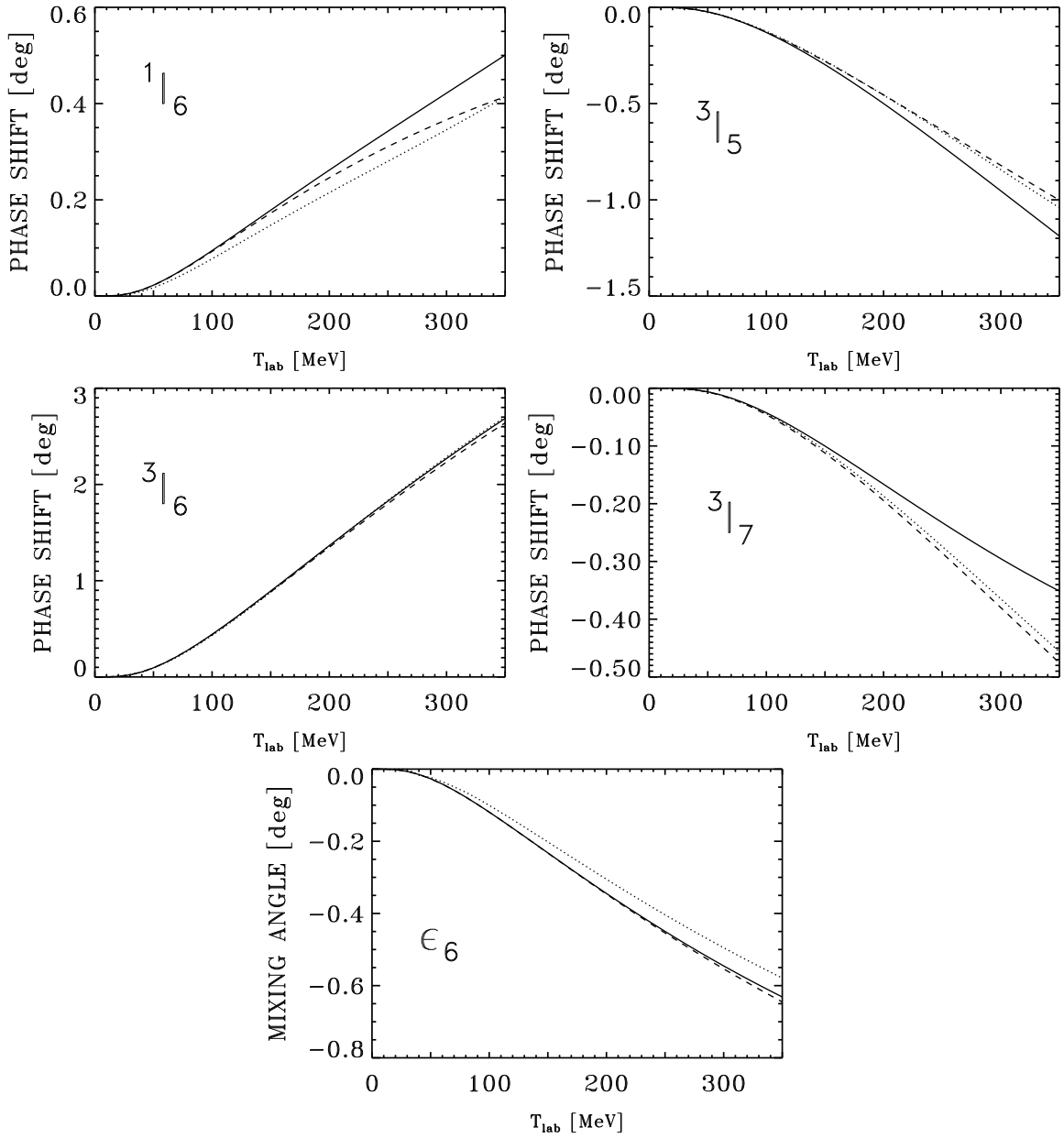

Fig.8: I-wave NN phase shifts and mixing angle ϵ_6 versus the nucleon laboratory kinetic energy T_{lab}. For notations see Fig.4.

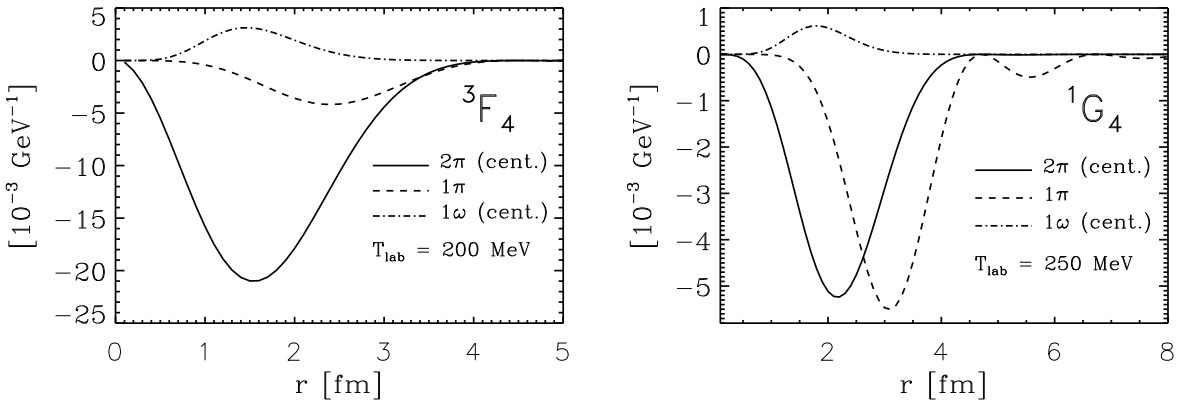

Fig.9: Examples of NN interaction densities in coordinate space. Dashed lines show the 1π-exchange contributions. Full and dashed-dotted curves give the isoscalar central components of 2π-and ω-exchange, respectively.

Acknowledgement

We thank V. Pandharipande for useful discussions.

APPENDIX: RELATIVISTIC 1/M-CORRECTION TO Δ-EXCITATION

Here we will collect explicit formulas for the first relativistic correction proportional to $1/M$ arising from the single and double Δ-excitation graphs in Fig.1. A convenient way to obtain these corrections is to use relativistic propagators and vertices and to perform the $1/M$-expansion inside the loop integral. For the $\Delta(1232)$ with spin-3/2 this requires the Rarita-Schwinger formalism which gives for the Δ-propagator

$$-\frac{i}{3}\frac{\gamma\cdot k+M_\Delta}{k^2-M_\Delta^2+i0^+}\Big\{3g_{\mu\nu}-\gamma_\mu\gamma_\nu-\frac{2k_\mu k_\nu}{M_\Delta^2}+\frac{k_\mu\gamma_\nu-k_\nu\gamma_\mu}{M_\Delta}\Big\} \tag{42}$$

and for the $\Delta\to\pi^a N$ transition vertex

$$\frac{3g_A}{2\sqrt{2}f_\pi}\Big(l^\mu+Z'\gamma\cdot l\,\gamma^\mu\Big)\,T_a\ . \tag{43}$$

Z' is an off-shell parameter lying within in the empirically determined band $-0.8<Z'<0.3$ [16]. Again, we omit here additive linear polynomials $c\,q^2+c'$ in the central amplitudes and additive constants in the tensor and spin-orbit amplitudes which contain the divergent pieces of the diagrams. We will give separately the contributions coming from the three classes of Δ-excitation diagrams. We present first the results for $Z'=0$ and then display additional Z'-dependent terms as far as they show up at order $1/M$.

a) $1/M$-correction to triangle graphs with Δ-excitation:

$$W_C=\frac{g_A^2\Delta}{192\pi^2Mf_\pi^4}\Big\{(4m_\pi^2+7q^2)L(q)+3\Sigma\,H(q)+3(4\Delta^2q^2-\Sigma^2)D(q)\Big\}\ , \tag{44}$$

$$W_{SO}=2W_T=-\frac{2}{q^2}\,W_S=\frac{g_A^2\Delta}{128\pi^2Mf_\pi^4}\Big\{-2L(q)+(w^2-4\Delta^2)D(q)\Big\}\ . \tag{45}$$

b) $1/M$-correction to box graphs with single Δ excitation:

$$V_C = \frac{3g_A^4}{128\pi^2 M f_\pi^4 \Delta}\Big\{2[q^4+2q^2m_\pi^2+2q^2\Delta^2+4m_\pi^4-8m_\pi^6 w^{-2}]L(q) \\ +(2m_\pi^2+q^2)^3\Delta^{-1}\pi A(q)+\Sigma\,[(2m_\pi^2+q^2)^2-4q^2\Delta^2]D(q)\Big\}\ , \tag{46}$$

$$W_C = \frac{g_A^4}{384\pi^2 M f_\pi^4 \Delta}\Big\{3(2m_\pi^2+q^2)^3\Delta^{-1}\pi A(q)+2\Delta^2(8m_\pi^2-q^2)L(q) \\ +3\Sigma^2\,H(q)+3\Sigma\,[(2m_\pi^2+q^2)^2+4\Delta^2(q^2-\Delta^2)]D(q\Big\}\ , \tag{47}$$

$$V_T = -\frac{1}{q^2}\,V_S = \frac{3g_A^4}{512\pi^2 M f_\pi^4 \Delta}\Big\{(2m_\pi^2+q^2)w^2\Delta^{-1}\pi A(q) \\ +\Sigma\,[2L(q)+(4\Delta^2+w^2)D(q)]\Big\}\ , \tag{48}$$

$$W_T = -\frac{1}{q^2}\,W_S = \frac{g_A^4}{512\pi^2 M f_\pi^4 \Delta}\Big\{(2m_\pi^2+q^2)w^2\Delta^{-1}\pi A(q) \\ +2(4\Delta^2+\Sigma)L(q)+\Sigma\,(w^2-4\Delta^2)D(q)\Big\}\ , \tag{49}$$

$$V_{SO} = \frac{3g_A^4}{256\pi^2 M f_\pi^4 \Delta}\Big\{-(2m_\pi^2+q^2)w^2\Delta^{-1}\pi A(q) \\ +2\Sigma\,[2L(q)+(4\Delta^2+w^2)D(q)]\Big\}\ , \tag{50}$$

$$W_{SO} = \frac{g_A^4}{256\pi^2 M f_\pi^4 \Delta}\Big\{2(2m_\pi^2+q^2)w^2\Delta^{-1}\pi A(q) \\ -2\Sigma\,L(q)+(4\Delta^2+\Sigma)(4\Delta^2-w^2)D(q)\Big\}\ . \tag{51}$$

Additional contributions for $Z' \neq 0$:

$$V_C = -\frac{3g_A^4 Z'}{32\pi M f_\pi^4}(3Z'+1)(2m_\pi^2+q^2)^2 A(q)\ , \tag{52}$$

$$W_T = -\frac{1}{q^2}\,W_S = \frac{g_A^4 Z'}{64\pi M f_\pi^4}(3Z'+1)w^2 A(q)\ . \tag{53}$$

c) $1/M$-correction to box graphs with double Δ-excitation:

$$V_C = \frac{g_A^4\Delta}{256\pi^2 M f_\pi^4}\Big\{4(5q^2-16m_\pi^2)L(q)-K(q) \\ +3[\Delta^{-2}\Sigma^3+8(q^4+6q^2m_\pi^2+2q^2\Delta^2+8m_\pi^4-8m_\pi^2\Delta^2)]D(q) \\ +3[\Delta^{-2}(2m_\pi^2+q^2)^2+4(2m_\pi^2+3q^2-3\Delta^2)]H(q)\Big\}\ , \tag{54}$$

$$W_C = \frac{g_A^4\Delta}{1536\pi^2 M f_\pi^4}\Big\{8(12\Delta^2-8m_\pi^2+q^2)L(q)-K(q) \\ +3[16(2\Delta^4-2m_\pi^4+3q^2\Delta^2-3q^2m_\pi^2-q^4)-\Delta^{-2}\Sigma^3]D(q) \\ +3[4(6m_\pi^2+5q^2-5\Delta^2)-\Delta^{-2}(2m_\pi^2+q^2)^2]H(q)\Big\}\ , \tag{55}$$

$$V_{SO} = 4V_T = -\frac{4}{q^2}\,V_S = \frac{3g_A^4}{512\pi^2 M f_\pi^4 \Delta}\Big\{8\Delta^2 H(q) \\ -\Sigma\,[2L(q)+(12\Delta^2+w^2)D(q)]\Big\}\ , \tag{56}$$

$$W_{SO} = 4W_T = -\frac{4}{q^2}\, W_S = \frac{g_A^4}{1024\pi^2 M f_\pi^4 \Delta}\Big\{2(\Sigma - 8\Delta^2)L(q) \\ +8\Delta^2 H(q) + (8\Delta^2 + \Sigma)(w^2 - 4\Delta^2)D(q)\Big\}\ . \tag{57}$$

Additional contributions for $Z' \neq 0$:

$$V_C = \frac{g_A^4 \Delta Z'}{16\pi^2 M f_\pi^4}\Big\{3\Sigma\,[2\Delta^2 - \Sigma - Z'(2\Delta^2 + 3\Sigma)]D(q) \\ +2[7m_\pi^2 + 4q^2 - 6\Delta^2 + Z'(13m_\pi^2 + 7q^2 - 6\Delta^2)]L(q)\Big\}\ , \tag{58}$$

$$W_T = -\frac{1}{q^2}\, W_S = \frac{g_A^4 \Delta Z'}{128\pi^2 M f_\pi^4}(3Z' + 1)\Big\{(w^2 - 4\Delta^2)D(q) - 2L(q)\Big\}\ . \tag{59}$$

The abbreviation $K(q)$ stands for

$$K(q) = \frac{48\,\Sigma^3}{(w^2 - 4\Delta^2)^2}\Big[L(q) - \frac{w^2 - 4\Delta^2}{4\sqrt{\Delta^2 - m_\pi^2}} L'(2\sqrt{\Delta^2 - m_\pi^2}) - L(2\sqrt{\Delta^2 - m_\pi^2})\Big]\ , \tag{60}$$

and we refer to eqs.(15-19) for the definition of the functions w, Σ, $L(q)$, $A(q)$, $D(q)$. Note that to order $1/M$ only the isoscalar central V_C and the isovector spin-spin/tensor $W_{S,T}$ NN-amplitudes depend on the uncertain off-shell parameter Z'. Some terms given above have a prefactor $g_A^4/(M f_\pi^4 \Delta^2)$ of dimension mass^{-7}. In coordinate space these terms will lead to a potential with a rather problematic r^{-8}-singularity near the origin.

In particular, we have calculated here for the first time the spin-orbit interaction (V_{SO}, W_{SO}) generated by 2π-exchange with Δ-excitation. These spin-orbit NN-amplitudes are truly relativistic effects (absent in the static limit and independent of Z') and they may be of interest in future studies of the NN spin-orbit interaction.

REFERENCES

[1] N. Kaiser, R. Brockmann and W. Weise, *Nucl. Phys.* **A625** (1997) 758.
[2] V. Bernard, N. Kaiser and Ulf-G. Meißner, *Nucl. Phys.* **A615** (1997) 483.
[3] R. Tarrach and M. Ericson, *Nucl. Phys.* **A294** (1978) 417; M. Ericson and A. Figureau, *J. Phys.* **G7** (1981) 1197.
[4] J.W. Durso, A.D. Jackson and B.J. Verwest, *Nucl. Phys.* **A345** (1980) 471.
[5] J.W. Durso, M. Saarela, G.E. Brown and A.D. Jackson, *Nucl. Phys.* **A278** (1977) 445.
[6] R.A. Smith and V.R. Pandharipande, *Nucl. Phys.* **A256** (1976) 327.
[7] A.M. Green, *Rep. Prog. Phys.* **39** (1976) 1109.
[8] R. Machleidt, K. Holinde and Ch. Elster, *Physics Reports* **149** (1987) 1 and references therein.
[9] G. Höhler, in Landolt-Börnstein, Vol.9b2, ed. H. Schopper, Springer-Verlag, 1983.
[10] C. Ordonez, L. Ray and U. van Kolck, *Phys. Rev.* **C53** (1996) 2086.
[11] D.B. Kaplan, M.J. Savage and M.B. Wise, *Nucl. Phys.* **B478** (1996) 629; and preprint nucl-th/9801034.
[12] V. Bernard, N. Kaiser and Ulf-G. Meißner, *Int. J. Mod. Phys.* **E4** (1995) 193.
[13] T.R. Hemmert, B.R. Holstein and J. Kambor, *Phys. Lett.* **B395** (1997) 89; and preprint hep-ph/09712496.
[14] T. Ericson and W. Weise, *Pions and Nuclei*, Clarendon Press, Oxford, 1988.
[15] R.D. Peccei, *Phys. Rev.* **176** (1968) 1812.
[16] M. Benmerrouche, R.M. Davidson and N.C. Mokhopadhyay, *Phys. Rev.* **C39** (1989) 2339.
[17] J. Gasser, H. Leutwyler and M.E. Sainio, *Phys. Lett.* **B253** (1991) 252, 260.
[18] V. Bernard, N. Kaiser and Ulf-G. Meißner, *Z. Phys.* **C60** (1993) 111.
[19] V. Bernard, N. Kaiser, J. Kambor and Ulf-G. Meißner, *Nucl. Phys.* **B388** (1992) 315.
[20] P. Mergell, Ulf-G. Meißner and D. Drechsel, *Nucl. Phys.* **A596** (1996) 367.
[21] W. Grein and P. Kroll, *Nucl. Phys.* **A338** (1980) 332; *Nucl. Phys.* **A377** (1982) 505.
[22] R.A. Arndt, J.S. Hyslop and L.D. Roper, *Phys. Rev.* **D35** (1987) 128; R.A. Arndt and L.D. Roper, Scattering Analysis Interactive Dial-in Program (SAID), Virginia Polytechnic Institute and State University.
[23] R. Dubois *et al. Nucl. Phys.* **A377** (1982) 554.
[24] V.G.J. Stoks, R.A.M. Klomp, M.C.M. Rentmester and J.J. de Swart, *Phys. Rev.* **C48** (1993) 792.
[25] J.L. Ballot, M.R. Robilotta and C.A. da Rocha, preprint nucl-th/9801022.